Chapter 1
Introduction to Transient Chaos

In numerical or experimental investigations one never has infinitely long time intervals at one's disposal. In fact, what is needed for the observation of chaos is a well-defined *separation of time scales*. Let t_0 denote the internal characteristic time of the system. In continuous-time problems, t_0 can be the average turnover time of trajectories on a Poincaré map in the phase space. In a driven system, it is the driving period. In discrete-time dynamics, t_0 can be the time step itself.

Suppose one observes signals that appear random for an *average lifetime* τ. Since chaos is characterized by a sensitive dependence on initial conditions, which is meaningful only on sufficiently long time scales, the appearance of chaotic signals requires that τ be much greater than the internal characteristic time:

$$\tau \gg t_0 . \tag{1.1}$$

The difference between sustained and transient chaos lies in the actual value of τ: for the former, τ is infinite, but it is finite for the latter. As a matter of practicality, one cannot exclude the possibility that a system apparently exhibiting a chaotic attractor may turn out to be transiently chaotic if a much longer period of observation is allowed. It is therefore useful to consider an additional time scale: the observation time T_{O}. The sustained or transient nature of chaos then depends on how τ is compared with T_{O}. We can speak of transient chaos if

$$\tau < T_{\mathrm{O}} . \tag{1.2}$$

In the numerical investigation of attractors, a general habit is to discard a long sequence of the trajectory in order to concentrate on the asymptotic properties. A much richer dynamics may be observed, however, if one follows the trajectories from the beginning, i.e., if transients are not thrown out. One often finds then complex dynamics over some time, different from the dynamics governed by the attractor. The lifetime of a chaotic transient depends on the initial condition. An example can be seen in Fig. 1.1, where transiently chaotic trajectories are shown from the Hénon map [325, 564] at a parameter set where the attractor is a limit cycle.

Such signals can also be observed in experiments. An example is shown in Fig. 1.2, where the measured quantity is the temperature difference between two

Y.-C. Lai and T. Tél, *Transient Chaos: Complex Dynamics on Finite-Time Scales*,
Applied Mathematical Sciences 173, DOI 10.1007/978-1-4419-6987-3_1,

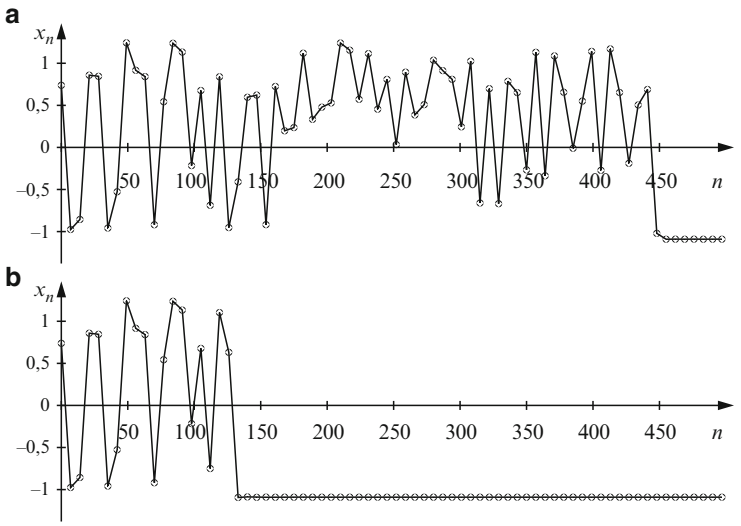

Fig. 1.1 Transient chaotic signals from the Hénon map $x_{n+1} = 1 - ax_n^2 + by_n$, $y_{n+1} = x_n$ for parameters $a = 1.25$ and $b = 0.3$, with a period-7 attractor. For clear visualization, only every seventh iterate is shown. (**a**) Trajectory initiated at $x_0 = 0.738816$, $y_0 = 0.893088$ exhibits chaotic behavior over 441 iterates. (**b**) The initial condition is shifted by $2 \cdot 10^{-19}$ in the x direction and the length of the chaotic transient is only 126

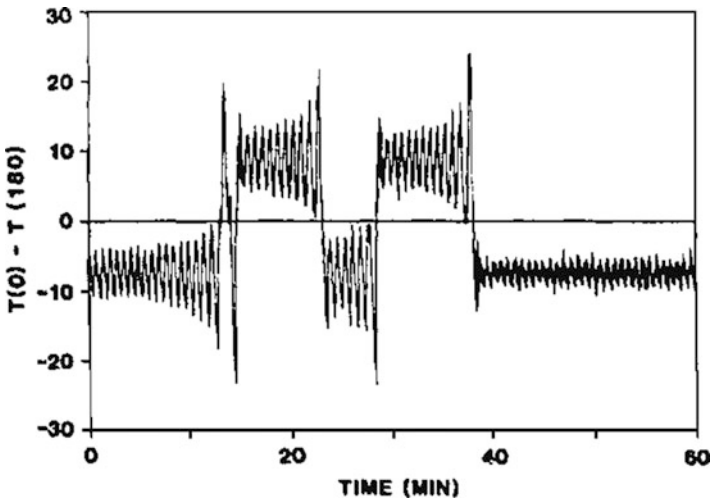

Fig. 1.2 Transient chaotic signal of the temperature difference observed between two points of an experimental loop of fluid heated from below with a constant heat flux (see Sect. 1.3 for more details). In this run, chaotic oscillations last up to nearly 40 min [823] (with kind permission from Elsevier Science)

points in a fluid loop. Over some time chaotic temperature oscillations are observed, which are accompanied by chaotic velocity oscillations of the laminar flow in the loop, and then, rather suddenly, a crossover takes place towards a nearly constant temperature difference corresponding to a uniform rotation of the fluid motion. (For a list of other representative experiments, see Sect. 1.3.)

Based on these and many other examples, one concludes that transiently chaotic signals (whose precise characterization will be discussed in Sect. 1.2) have the following characteristic properties:

1. For a fixed initial condition the signal appears chaotic up to certain time and then switches over, often quite abruptly, into a different, often nonchaotic, behavior that governs all the rest of the signal. The average lifetime, τ, can be obtained from an ensemble of such observations, although for individual observations, the actual lengths of transients depend sensitively on initial conditions: nearby trajectories typically have drastically different lifetimes.
2. The probability *distribution*, $P(t)$, of finding lifetimes longer than t is a smooth function, which satisfies $P(t) \to 0$ for $t \to \infty$.
3. There exist infinitely long transients. Mathematically, however, the set of initial conditions leading to infinite transients has zero volume in the phase space (has Lebesgue measure zero). Physically, this means that such infinite transients cannot be realized by initial conditions chosen randomly. In fact, for a typical (i.e., randomly chosen) initial condition, the transient lifetime is finite. Nonetheless, it is the presence of the measure-zero set of the initial conditions with infinite transients which causes the random distribution of the transient lifetimes for typical initial conditions.
4. It is known [564] that in a parameter region where chaotic attractors arise, periodic windows are dense. That is, for a specific parameter value that leads to a chaotic attractor, an arbitrarily small perturbation in the parameter can lead to a periodic attractor. In this sense, chaotic attractors are not structurally stable. Transient chaos is, however, robust against small parameter perturbations.

Similar to the fact that sustained chaotic signals are due to chaotic attractors in the phase space, there exist chaotic invariant sets that are responsible for transiently chaotic signals. Globally, such a chaotic set does not attract trajectories from its neighborhood, and hence it is *nonattracting*. Nonattracting chaotic sets (chaotic saddles or repellers; see Sect. 1.1.2) are therefore the *phase-space objects* that underly transient chaos. We thus accept the following definition: *transient chaos is the form of chaos due to nonattracting chaotic sets in the phase space*.

This chapter serves as a "first acquaintance" with transient chaos. The basic properties of nonattracting chaotic sets will be described. The average lifetime and the *escape rate* from these sets will then be introduced. Different methods for numerically constructing nonattracting chaotic sets will be given. The construction of the *natural* probability distribution on these sets will also be discussed, and an important related distribution, the *conditionally invariant measure* (c-Measure), will be introduced, from which characterizing quantities such as the Lyapunov exponents of the transients and dimensions of the nonattracting chaotic sets can be defined

and calculated. To underline the scientific relevance of transient chaos, a list of experiments taken from different disciplines will be presented, which also illustrate different aspects of transient chaos. Finally, a brief history of transient chaos will be given.

1.1 Basic Notions of Transient Chaos

1.1.1 Dynamical Systems

Dynamical systems are usually described by a set of ordinary differential equations:

$$\frac{\mathrm{d}\mathbf{x}}{\mathrm{d}t} = \mathbf{F}(\mathbf{x}, p), \tag{1.3}$$

where $\mathbf{x}(t)$ is the vector characterizing the state of the system at time t and p represents a set of parameters. Alternatively, discrete-time dynamical systems, or maps, of the form

$$\mathbf{x}_{n+1} = \mathbf{f}(\mathbf{x}_n, p) \tag{1.4}$$

can be investigated, where $\mathbf{x}_n$ is the state vector at discrete time n. Unless otherwise stated, the map is assumed to be autonomous, i.e., $\mathbf{f}$ does not depend explicitly on n. Maps can always be deduced from flows (1.3) by taking an appropriately defined Poincaré surface of section or stroboscopic map [564], the latter corresponding to repeatedly taking snapshots of the system at the multiples of some characteristic time t_0. Using such maps, the phase-space dimension is reduced effectively by one, facilitating visualization and analysis. In fact, Poincaré or stroboscopic maps have been used commonly in numerical and laboratory experiments on transient chaos (see Sect. 1.3). In order to have a consistent terminology, maps will be used for the rest of the chapter to illustrate the basic dynamical properties of transient chaos, but the main results apply also to flows (see also [398]).

1.1.2 Saddles and Repellers

The actual form of a nonattracting chaotic set depends on whether the dynamics is invertible. A dynamical system is invertible if its motion can be uniquely followed when time is reversed. This does not imply, however, that the time-reversed dynamics can actually occur in reality (although this is true for Hamiltonian systems, which are invariant under time reversal if no external magnetic field or Coriolis effect is present). Dynamical systems described by differential equations are typically invertible due to the uniqueness of solutions. Invertible dynamical systems are thus physically relevant. Noninvertible systems such as those described by one-dimensional maps can, however, be quite useful models for understanding specific features of transient chaos, and we shall consider them as well.

In an invertible dynamical system, a typical nonattracting chaotic set repels trajectories only along some special hypersurface in the phase space, which is called the *unstable manifold*. Along a different invariant hypersurface, or the *stable manifold*, the set can actually attract nearby trajectories. Usually, the local phase space at a point in the chaotic set can be decomposed into the stable and the unstable subspaces. For this reason, nonattracting chaotic sets in invertible dynamical systems are called *chaotic saddles*. Because differential equations are, in general, invertible, and many real-life phenomena are described by differential equations, *transient chaos in experiments is typically related to chaotic saddles*.

In contrast, for noninvertible dynamical systems in which the inverse is not unique, nonattracting chaotic sets are often *chaotic repellers*, objects that are repellent in all possible directions of the phase space. Chaotic repellers possess only unstable manifolds. These considerations are summarized in Table 1.1. The geometrical appearances of chaotic saddles and chaotic repellers can be quite different, as Fig. 1.3 illustrates.

The dynamical difference between chaotic repellers and saddles is that long-lived trajectories can start only from a neighborhood of the repeller, but for saddles

Table 1.1 Types of typical nonattracting chaotic sets in nonlinear dynamical systems

Dynamics	Nonattracting chaotic set
Invertible	Chaotic saddle
Noninvertible	Chaotic repeller

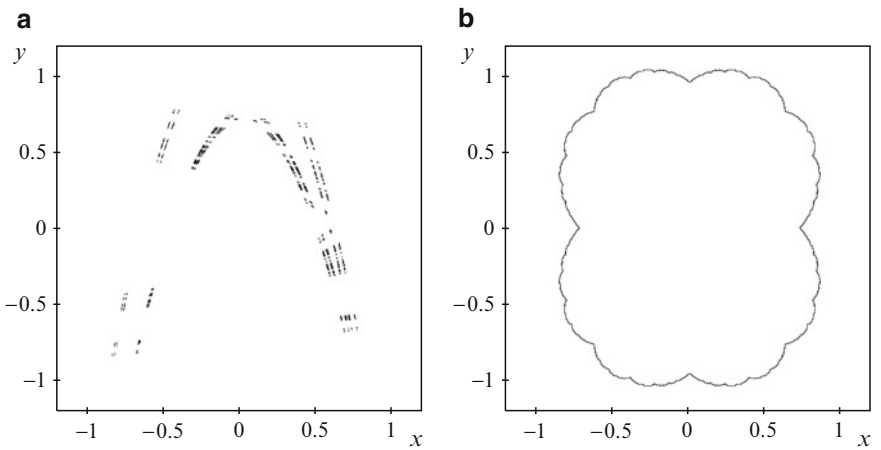

Fig. 1.3 Comparison of a chaotic saddle and a chaotic repeller. (**a**) A chaotic saddle from a periodically kicked harmonic oscillator. On a stroboscopic plane the position x_n and the velocity y_n of the oscillator evolve according to the map [773] $x_{n+1} = y_n$, $y_{n+1} = 1 - 3.2y_n^2 - 0.49x_n$. (**b**) A chaotic repeller of the quadratic map $z_{n+1} = {z_n}^2 + 0.2$ in the complex plane $z = x + iy$, which is in fact a Julia set [824]. The saddle in (**a**) appears as a fractal set of points, which is in fact the direct product of two Cantor-like sets, while the repeller in (**b**) is a complicated but nonetheless continuous curve in the plane

they can also start from a neighborhood of the stable manifold, a typically much larger set. If a chaotic repeller and saddle coexist,[1] transient chaos is primarily governed by the chaotic saddle.

Because a nonattracting chaotic set is invariant, trajectories starting from points on the set *never* leave the set and in fact exhibit chaotic motion for infinitely long time. However, because the Lebesgue measure of the set is zero, the probability that a randomly chosen point of the phase space is in the set is zero. What is *observable* is not the nonattracting set but a a *small neighborhood* of it. In particular, trajectories can originate from points in the vicinity of the set and can then stay in the neighborhood of the set for a long but finite amount of time, and they eventually leave the nonattracting chaotic set. These are the trajectories that generate transiently chaotic signals. The phenomenon of transient chaos thus illustrates that the existence of a set of Lebesgue measure zero can be observed via *finite-time properties*. As a consequence, we shall also see that the fractal features of a nonattracting chaotic set are different from those of a chaotic attractor.

A related point is that the natural measure, a special invariant distribution characterizing the dynamics on a nonattracting chaotic set, not only exists but can be obtained approximately in numerical or actual experiments. In particular, the distribution can be approximately specified on a small neighborhood of the set. The approximate natural measure can then be used to perform *ensemble averages* of physical quantities of interest, similar to the situation with chaotic attractors. Since the distribution is only approximate, any ensemble average will contain errors, but they can be controlled.

Transient chaotic dynamics can also be classified according to whether the process is dissipative or conservative. In a strictly dissipative system where the local phase-space volume contracts everywhere, the asymptotic states of the system are attractors that may be regular, but transient chaos provides a "platform" for approaching the attractors. In such a case the transient dynamics before the final state of the system is reached is chaotic. In *dissipative* systems, transient chaos appears in the form of *chaotic transients*. In conservative or Hamiltonian systems, the phase-space volume is constant under time evolution. As a result, there are no attractors, but some simple asymptotic states of the system can still be defined. Consider, for example, a particle-scattering experiment in which the underlying dynamics is Hamiltonian. Particles coming from far away approach the scattering region, and after a finite amount of time, they leave the region and escape to "infinity." There can, however, be qualitatively different exit routes to infinity. In this case, the different exit routes can be regarded as asymptotic states (but not attractors) of the system. The dynamics in the scattering region can, however, be regular or chaotic, where the latter, i.e., transient chaos in *Hamiltonian systems*, defines the phenomenon of *chaotic scattering*. Hamiltonian systems are invertible, so the nonattracting set underlying chaotic scattering is typically a saddle.

[1] For instance, in the time-reversed dynamics of an invertible system possessing a chaotic attractor and a coexisting chaotic saddle.

It should be noted that *nonchaotic transients* may also exist in dynamical systems. An example is provided by trajectories that approach an attractor but are far away from any nonattracting chaotic set. These transients are typically short and do not exhibit chaotic features, although the actual asymptotic state may be chaotic. Thus, *transients to chaos* can be quite different from chaotic transients, since the latter, but not the former, are due to an underlying nonattracting chaotic set.

1.1.3 Types of Transient Chaos

According to the type of attractor(s) with which a nonattracting chaotic set coexists, we can distinguish two main types of transient chaos. The first type is for the case in which the coexisting attractor is simple, e.g., a periodic attractor. While the asymptotic behavior of the system is relatively simple, the transients are chaotic. Transient chaos arising in situations in which there is an attractor at infinity, and in open Hamiltonian systems in which attractors are replaced by different exit routes also exhibit this type of transient chaos.

The second type occurs when a nonattracting chaotic set coexists with a chaotic attractor. In this case, there are two distinct forms of chaotic behavior. A signal from the system typically exhibits one form of chaotic behavior, the one due to the nonattracting set, on time scale τ, and then switches over to another form of chaos asymptotically. A common situation is that the motion determined by the nonattracting set is more chaotic than that due to the chaotic attractor (for more detail see Fig. 1.16 and Chap. 3). Thus, focusing on the asymptotic properties will "miss" the dominant chaotic part of the full complex dynamics that contains important information about the underlying dynamical system.

1.2 Characterizing Transient Chaos

Having introduced the basic concepts of transient chaos in a qualitative manner, we now discuss its quantitative characterization. A natural question is whether there is actually chaos in the seemingly chaotic signals observed over finite time scales. There are different levels of characterization of increasing complexity, as follows:

1. Measurement of the lifetime distribution, the escape rate, and the average lifetime.
2. Construction of nonattracting chaotic sets in the phase space.
3. Construction of invariant measures on the chaotic set.
4. Determination of dynamical invariants such as the Lyapunov exponents and the fractal dimensions of the nonattracting chaotic set and its natural measure.

Following this hierarchy, one can find criteria to address the question of whether the system is indeed chaotic and if so, to calculate some measure of the strength of chaoticity. In the following we discuss these levels of characterization.

1.2.1 Escape Rate

In transient chaos, typical trajectories, i.e., trajectories initiated from random initial conditions, escape any neighborhood of the nonattracting chaotic set. A quantity measuring how quickly this occurs is the *escape rate* [824]. To define the escape rate, imagine distributing a large number N_0 of initial points according to some initial density ρ_0 in a phase-space region R that does not contain any attractor or asymptotic state of the system. The density ρ_0 is often chosen to be uniform, and the geometry of R can be chosen to be simple, e.g., a rectangle in a two-dimensional phase space. Many trajectories from the initial points may come close to the nonattracting chaotic set at some later time. We define a *restraining region* Γ as a bounded, compact region containing the nonattracting set. Once a point leaves the restraining region, it cannot return to it. After visiting a neighborhood of the set, almost all trajectories eventually leave Γ. Let $N(n)$ denote the number of trajectories remaining inside Γ after n steps, and choose N_0 to be sufficiently large that $N(n) \gg 1$. As n is increased, one observes in general an exponential decay in the number of trajectory points that are still in Γ (surviving points) [373, 596, 843]:

$$N(n) \sim \mathrm{e}^{-\kappa n} \quad \text{for} \quad n \gg 1, \tag{1.5}$$

where κ is called the escape rate.[2] A small value of κ implies weak "repulsion" of typical trajectories by the nonattracting chaotic set. The escape rate turns out to be *independent* of the distribution ρ_0 of the initial conditions, of its support R, and of the choice of the restraining region Γ. The escape rate κ is thus a property *solely* of the nonattracting chaotic set. However, the prefactor of the exponential form in (1.5), and the behavior of the system preceding the exponential decay do depend on details such as the choices of ρ_0, R, and Γ.

A practical issue concerns about the choice of the support R of the initial density. In a noninvertible system, R should overlap with the chaotic repeller, while in an invertible system it is sufficient to choose R so that it overlaps with the stable manifold of the chaotic saddle. In any case, if an exponential decay is found, its rate should be given by the escape rate κ. In practice, the initial density is often distributed on the restraining region, implying $R = \Gamma$.

In a realistic physical system, the exponential decay can be observed with high accuracy after a finite, often short, time n^*, i.e.,

$$N(n) = N\mathrm{e}^{-\kappa n} \quad \text{for} \quad n \geq n^*, \tag{1.6}$$

[2] There are situations in which the decay follows a power law for certain types of nonhyperbolic chaotic sets, which will be treated in Sect. 2.4 and Chap. 6. Such decays cannot be characterized by escape rates.

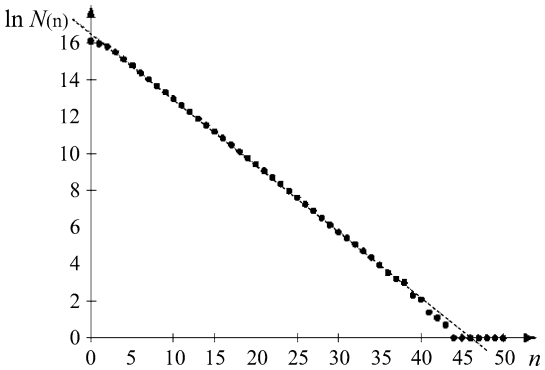

Fig. 1.4 Survival in the Hénon map $x_{n+1} = 1 - ax_n^2 + by_n$, $y_{n+1} = x_n$ for parameters $a = 2.0$ and $b = 0.3$. Number $N(n)$ of surviving trajectory points in the square defined by $\Gamma : |x_n|, |y_n| \leq 1.0$, obtained from $N_0 = 10^6$ initial points distributed uniformly in the same square ($R = \Gamma$). The fitted *dashed line* has slope approximately -0.36, giving $\kappa \approx 0.36$. The value of n^* is approximately 4. The survival probability $P(n)$ is approximately $N(n)/N_0$

where the value of n^* and the prefactor N may also depend on ρ_0, R, and Γ.[3] An example is shown in Fig. 1.4, where we see that the value of n^* is relatively small.

The definition of the escape rate indicates that the number of surviving points is decreased by a factor of $1/e$ after about $1/\kappa$ time steps. This implies that most trajectories do not live longer than $1/\kappa$ in the restraining region. It is thus reasonable to *estimate* the average lifetime τ of the chaotic transient as

$$\tau \approx \frac{1}{\kappa}. \tag{1.7}$$

Since the escape rate can be obtained by following the decay law over a finite time interval, cf. (1.5), transient chaos of short average lifetime may be difficult to identify. A condition for the practical observability of transient chaos is thus that κ be small.

In a more general context, for any initial distribution on R and choice of Γ, we can define the *probability* $P(n)$ of finding survival times larger than $n \geq 1$. The *survival probability* $P(n)$ is thus the probability of finding initial points that have not escaped Γ up to time n, which can be approximated by $N(n)/N_0$ for large N_0. In view of (1.6), the decay of $P(n)$ is exponential:

$$P(n) = g\mathrm{e}^{-\kappa n} \quad \text{for} \quad n \geq n^*. \tag{1.8}$$

[3] The prefactor N yields what the number of initial points would be if the decay were exponential from the very beginning. Therefore N is different from N_0.

A related probability is the *escape-time distribution*, $p(n)$, the probability that a particle escapes region Γ exactly in the nth iterate. This quantity can be estimated as $[N(n-1)-N(n)]/N_0$ and is therefore the "density" of the cumulative distribution $P(n)$. We have

$$P(n) = \sum_{n'=n+1}^{\infty} p(n'). \tag{1.9}$$

Being the "derivative" of an exponential function, the long-time behavior of $p(n)$ is also exponential and can be written in the form of (1.8) (with a different n^*, but the *same* escape rate).[4]

The average lifetime τ is *defined* as the average escape time, i.e.,

$$\tau \equiv \bar{n} = \sum_{n=1}^{\infty} np(n). \tag{1.10}$$

Since the distribution is not exponential for $n < n^*$, the exact average lifetime τ *does* depend on the choices of ρ_0, R, and Γ. Note that the estimate (1.7) does not reflect this property.[5] Since the average lifetime depends on many details, the escape rate κ is a *more appropriate characteristic* of the decay process than τ. The escape rate is a unique property of the underlying nonattracting chaotic set, in contrast to the average lifetime, which also contains information about, e.g., the initial distribution of particles. While the values of τ and $1/\kappa$ are typically different even for slow decays, their *scaling properties* in terms of, for example, parameter changes are usually the same.

There can be situations in which two (or more) nonattracting chaotic sets coexist with different escape rates κ_1 and κ_2. In such a case, the number of surviving trajectory points in a given restraining region Γ is the sum of two exponentials for large n:

$$N(n) \sim N_1 \mathrm{e}^{-\kappa_1 n} + N_2 \mathrm{e}^{-\kappa_2 n}, \tag{1.11}$$

and the prefactors N_i depend on the choices of ρ_0, R, and Γ.

It should be emphasized that the existence of a positive escape rate κ for transients does not at all imply their chaoticity. One should also measure, for example, the Lyapunov exponents on time scale $1/\kappa$ [714] and check whether at least one of the exponents is positive. A complication is that even simple nonattracting sets, for instance a *single, regular saddle point* (also called a hyperbolic point) are at least partially repelling. Trajectories deviate from them exponentially. Regular

[4] For continuous-time systems, (1.5)–(1.8) remain valid under the transform $n \to t$. The escape-time distribution becomes then a probability density, and the sum in (1.9) is replaced by an integral. The escape rate in the corresponding continuous-time system is κ/t_0, where t_0 denotes the internal characteristic time mentioned in the introduction to this chapter. Analogously, the average lifetime can be estimated as t_0/κ.

[5] Equation (1.7) is a rough estimate, since even in the ideal case of $n^* = 1$, when $p(n) = (\exp(\kappa)-1)\exp(-\kappa n)$, we obtain $\tau = (1-\exp(-\kappa))^{-1}$ from (1.10) [147], which is consistent with (1.7) for $\kappa \ll 1$ only.

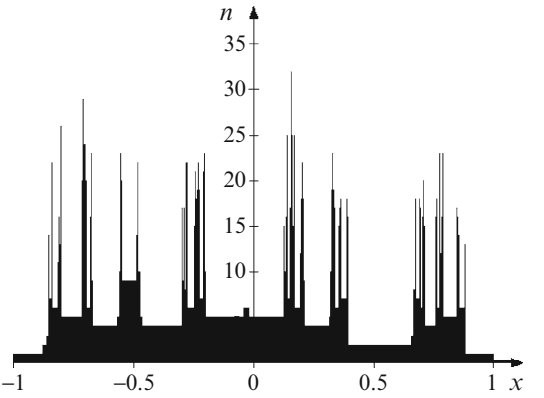

Fig. 1.5 Lifetime function: dependence of the lifetime n on the initial position x along the interval defined by $y = -1.5$ and $|x| \leq 1$ in the Hénon map at the parameters of Fig. 1.4. (For the corresponding phase-space patterns, see Figs. 1.7 and 1.9.) The fractal irregularity of this lifetime function is a sign of transient chaos

nonattracting sets are therefore characterized by a positive Lyapunov exponent, although the dynamics about them are not chaotic. The positivity of at least one Lyapunov exponent is thus not sufficient for the chaotic behavior of transients. This is why we accept the definition, used throughout the book, that transient chaos is the dynamics associated with nonattracting chaotic sets.

To determine whether the transients are truly chaotic, one therefore needs more information than the mere positivity of the Lyapunov exponent. Qualitatively, the visual appearance of the signal can be helpful: about chaotic nonattracting sets trajectories should be complicated. This is, nonetheless, only a hint. A property uniquely indicating the chaotic nature of the transients is the *irregular* dependence of lifetimes on initial conditions, as illustrated by Fig. 1.5. Suppose one starts trajectories along a smooth curve in the phase space that intersects a chaotic repeller or the stable manifold of a chaotic saddle. One then finds that for some points the lifetimes are large. In principle, points of infinitely large lifetimes belong to a *fractal* subset of initial conditions, since these must be points of the chaotic repeller or of the saddle's stable manifold. A fingerprint in a finite-accuracy numerical simulation is large lifetimes separated by small values in between.

1.2.2 Constructing Nonattracting Chaotic Sets

Repellers are straightforward to construct, since they are the attractors of the inverted dynamical systems. Noninvertibility is generally due to the existence of more than one inverted branch. When following the time-reversed dynamics, all possible inverses should be taken into account.

For an invertible dynamical system, the calculation of chaotic saddles is more delicate. While such a system can be inverted, the inverted dynamics still results in a chaotic saddle. This feature can in fact be viewed as an illustration of the robustness of the *hyperbolic structure* that is often seen for chaotic saddles. Roughly, a chaotic saddle is the set of intersections between the stable and the unstable manifolds, and

in hyperbolic cases, the angles at the intersecting points are bounded away from zero. In what follows, we will describe an intuitive numerical procedure for calculating chaotic saddles, which serves to further illustrate their dynamical structures. More practical numerical methods will then be introduced.

1.2.2.1 Horseshoe Construction

The intuitive method is based on the observation that a chaotic saddle has typically embedded within itself a dense set of unstable periodic orbits, a property of any chaotic set. Imagine that we choose an unstable periodic orbit in an invertible two-dimensional map and plot its stable and unstable manifolds, which are the curves along which the orbit is attracting in the direct and in the inverted dynamics, respectively. If these curves cross each other once at a point (a homoclinic point), they must do so infinitely many times, since the images and the preimages of such an intersection are of the same type. All the homoclinic points form a *homoclinic orbit*. Since it belongs simultaneously to the stable and the unstable manifolds of the original periodic orbit, a homoclinic orbit approaches asymptotically, but can never reach, the periodic orbit. As a result, the stable and unstable manifolds exhibit a complex, intertwined structure, as shown schematically in Fig. 1.6. The *horseshoe* structure of the manifolds and the existence of homoclinic orbits have been known since the works of Smale [300, 721]. Thus, mathematically, chaotic saddles are closed, bounded, and invariant sets with dense orbits. They are the "soul" of chaotic dynamics [721]. Similar to the formation of homoclinic orbits, the stable (unstable) manifold of a periodic orbit can intersect with the unstable (stable) manifold of a *different* orbit, forming a *heteroclinic orbit*. The stable and the unstable manifolds of different periodic orbits of a chaotic saddle are usually close to each other in the phase space, and all the resulting homoclinic and heteroclinic orbits belong to the chaotic saddle.

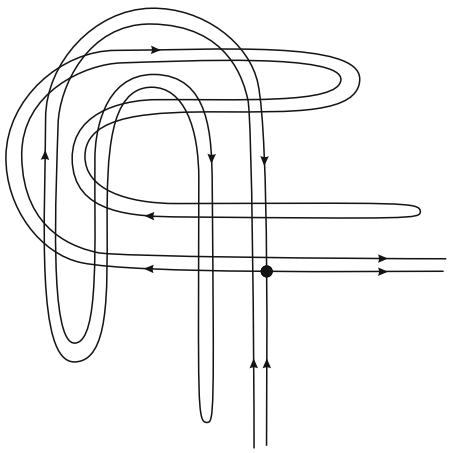

Fig. 1.6 Horseshoe structure: schematic illustration of horseshoes formed by the stable and the unstable manifolds of a fixed point (period-1 orbit) denoted by the *dot*. The set of intersection points (homoclinic points) between the manifolds belongs to the chaotic saddle

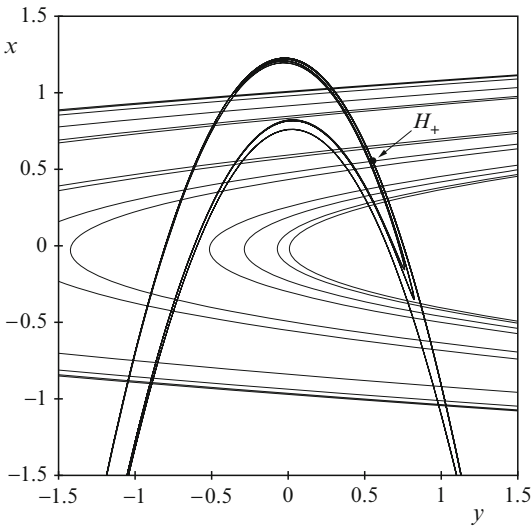

Fig. 1.7 A horseshoe construction: a few branches of the stable and the unstable manifolds of the fixed point H_+ of the Hénon map $x_{n+1} = 1 - 2.0x_n^2 + 0.3y_n$, $y_{n+1} = x_n$

The above discussion suggests the following procedure for numerically calculating a chaotic saddle. One first finds a simple hyperbolic orbit, such as a fixed point or a periodic orbit of low period, and then calculates its stable and unstable manifolds. In particular, the unstable (stable) manifold can be obtained by distributing a large number of initial points in a small neighborhood of the hyperbolic orbit and iterating them under the forward (inverted) dynamics. The set of intersecting points between the manifolds is part of the chaotic saddle. Since in practice, only a finite number of branches of the manifolds can be constructed, the intersections provide an approximate representation of the saddle. If the number of initial points used in the calculation is reasonably large, the fractal nature of the saddle and its stable and unstable manifolds can be revealed. An example is shown in Fig. 1.7. In general, the appearance of a fractal geometry along both the stable and the unstable manifolds and the existence of a horseshoe type of structure are indications that a chaotic saddle exists in the phase space of interest. Note that if the manifolds of the hyperbolic orbit chosen do not intersect each other, the orbit does not belong to a chaotic saddle. In this case, it is necessary to choose a different periodic orbit to start with.

1.2.2.2 Ensemble Method

The idea of this method, introduced by Kantz and Grassberger [380], is to follow an ensemble of trajectories and select the pieces that remain in the vicinity of the saddle. In particular, one first chooses a region R close to the suspected chaotic saddle but not containing any attractor, distributes uniformly a large number N_0 of points in R, and iterates these initial conditions under the forward dynamics. A criterion is needed for deciding when a trajectory is away from the saddle, which can simply be that the trajectory moves out of a restraining region Γ surrounding the

saddle (regions R and Γ can be the same as the respective ones used for computing the escape rate). Another criterion can be [380] to calculate the effective Lyapunov exponents over a finite number of time steps and examine whether they are close to the corresponding exponents characterizing an attractor. In the case of a point attractor, it is simply the negativity of all local Lyapunov exponents that can be used as an indicator of the trajectory's having left the saddle. All trajectories leaving the saddle earlier than n_0 steps are discarded, and trajectories of lifetime longer than or equal to n_0 are kept. The choice of the value of n_0 can be somewhat arbitrary, but some large value should be chosen if the lifetime τ of the chaotic saddle is large. (Experience indicates that choosing n_0 a few multiples of $1/\kappa$ is proper.) One can then select *long-lived* trajectories in the neighborhood of the saddle to approximate it. For example, if the desirable number of trajectories whose lengths are not less than n_0 is M_0, the number N_0 of initial points should be of the order of $n_0 M_0 \exp(\kappa n_0)$, which can be a few orders of magnitude larger than M_0. To ensure that trajectories close to the saddle are selected, the long-lived trajectories need to be *truncated* at both the beginning and the end. For example, for a trajectory of length larger than n_0, one can discard the first n_1 and the last n_2 points so that the resulting trajectory is close to the saddle but not close to its stable and unstable manifolds, respectively, where n_1 and n_2 are each a fraction of n_0. A representative example is shown in Fig. 1.8.

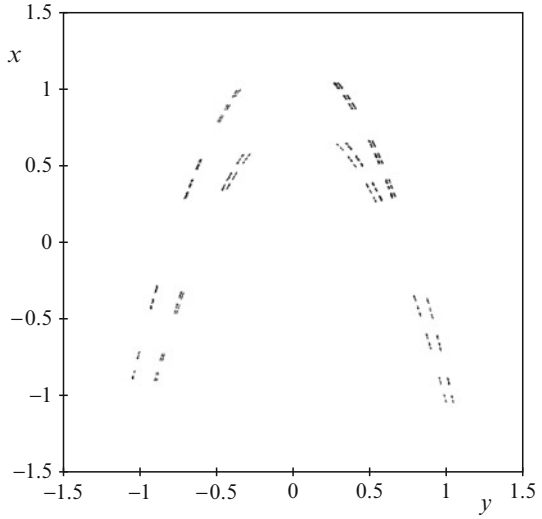

Fig. 1.8 Chaotic saddle in the Hénon map ($a = 2.0$, $b = 0.3$) obtained by the ensemble method, where $N_0 = 10^6$ initial points are distributed uniformly in the interval $R = (\mid y_0 \mid < 0.5,\ x_0 = 0)$. The restraining region is $\Gamma = \mid x_n \mid \leq 1.2$. The first 10 and the last 20 steps of long-lived trajectories are discarded ($n_0 = 30$). Observe that the pattern is practically the same as the one formed by the set of homoclinic points in Fig. 1.7. The direct product structure of two Cantor-like sets is a generic characteristic of chaotic saddles of two-dimensional maps

1.2.2.3 Sprinkler Method

A variant of the ensemble method, the *sprinkler method* [341], can be used to calculate not only a chaotic saddle but also its stable and unstable manifolds [453]. Again, one starts from $N_0 \gg 1$ trajectories distributed uniformly over a region R enclosing at least a part of the saddle. One then chooses an iteration number n_0 that is several times larger than the estimated lifetime (1.7) of the saddle, and follows the time evolution of each initial point up to exactly time n_0. Only trajectories that do not escape R in n_0 steps are kept, whose number is approximately $N_0 \mathrm{e}^{-n_0\kappa}$. If $n_0\kappa$ is sufficiently large (but not so large that only a few points remain inside R), trajectories with this long lifetime come close to the saddle in the course of dynamical evolution, implying that their initial points will be in the immediate vicinity of the stable manifold of the saddle, or of the saddle itself, and that their end points will be close to the unstable manifold of the saddle. The latter is so because most points still inside after n_0 steps might already be in the stage of leaving the region. The points from the middle of these trajectories (with $n \approx n_0/2$) are then in the vicinity of the saddle. In general, the initial, middle, and end points of trajectories of lifetimes of at least n_0 approximate the stable manifold, the saddle, and the unstable manifold, respectively, within the region R, as exemplified by Fig. 1.9. In order to obtain the full saddle, R should be chosen to fully contain the saddle (which corresponds to the choice $R = \Gamma$ in the ensemble method). An advantage of the sprinkler method is that it is computationally fast and is easy to apply to high-dimensional cases.

1.2.2.4 Single-Trajectory (PIM-Triple) Method

The PIM-triple method, proposed by Nusse and Yorke [557], sets out to find a single and arbitrarily long trajectory very much near the chaotic saddle. The procedure is

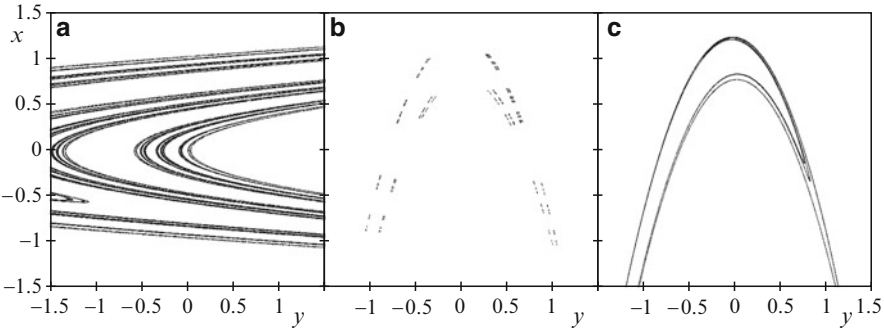

Fig. 1.9 Sprinkler method: an example of finding the chaotic saddle and its manifolds for the Hénon map in Figs. 1.7 and 1.8 by the sprinkler method. Region $R = \Gamma$ is a square of size 2×2 centered at the origin, $N_0 = 10^7$, $\kappa = 0.36$. Parts (**a**), (**b**), and (**c**) show points of trajectories with a minimum lifetime $n_0 = 16$ at iteration numbers $n = 0$, $n = 8$, and $n = 16$, well approximating the stable manifold, the saddle, and the unstable manifold, respectively. Note that the stable manifold here shows a more detailed structure than in Fig. 1.7

based on the observation that trajectories starting close to the *stable* manifold of the saddle stay for a long time in the vicinity of the saddle. The closer they start out to the stable manifold, the longer their lifetime is. One begins by taking an interval $\overline{AB}$ somewhere in a restraining region Γ so that it intersects the stable manifold of the chaotic saddle. One next chooses initial points uniformly distributed on $\overline{AB}$ and measures their lifetimes in Γ. A triplet of points, i.e., three points on $\overline{AB}$ such that the midpoint has a lifetime longer than those of the two neighboring points, can then be identified. Such a triplet is called a PIM-triple, where "PIM" stands for *proper interior maximum*. For the PIM-triple whose middle point has the maximum lifetime, the two external points are expected to lie on two different sides of a branch of the stable manifold. These two points then define a new interval $\overline{A'B'}$ that intersects the stable manifold. One can then repeat this *refining* procedure to find a PIM-triple whose size is smaller than a prescribed value $\delta \ll 1$. The triple can then be iterated forward under the dynamics. Points on the triple approach the saddle along the stable manifold but simultaneously move apart along the unstable manifold. When the size of the evolving triplet becomes larger than δ, the refining procedure is activated to reduce the size of the triple to within δ, and the new triple is iterated forward again, and so on. One thus finds a set of PIM-triples of size less than δ, and the set of middle points can be taken as an approximation of a typical trajectory on the chaotic saddle. While the PIM-triple procedure is computationally expensive (as compared with the previous methods), it is applicable to chaotic saddles even with relatively short lifetimes. The desirable feature of the PIM-triple method is that it enables a *long* trajectory near the saddle to be found, facilitating characterizations of the saddle by dynamical invariants such as the Lyapunov exponents and the fractal dimensions.

On a given interval, several PIM-triples can usually be found. If one selects from those the PIM-triple for which the lifetime at the middle is the largest, not only can the geometry of the saddle be revealed, but such a long trajectory also generates a good approximation to the natural measure on the saddle [353].

1.2.3 The Invariant Measures of Transient Chaos

1.2.3.1 Natural Measure

The natural measure (or natural invariant distribution) μ characterizes how often different pieces of a nonattracting chaotic set are visited by a dense trajectory on the set [380]. This distribution can be obtained from a *smooth* distribution about the set by selecting long-lived trajectories on the set. In practice, however, infinitely long trajectories cannot be found, nor can such trajectories be calculated with arbitrarily high precision. It is thus necessary to approximate the natural measure. For example, one can choose a fine but finite *coverage* of the chaotic set by boxes is the phase space of dimensionless linear size $\varepsilon \ll 1$, and consider trajectory points that stay for a long time close to the set.

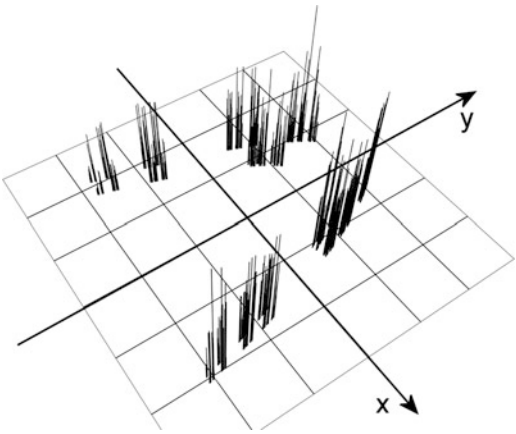

Fig. 1.10 Distribution of the natural measure μ of the Hénon chaotic saddle in Fig. 1.8 in a two-dimensional region in the phase space, specified on a grid of size $\varepsilon = 1/400$ (Picture by M. Gruiz and Sz. Hadobás)

Let N be the number of such points. All nonempty boxes define a *coarse-grained* version of the chaotic set at the resolution ε. The approximate natural measure on this coarse-grained set is given by the frequencies of visits to different boxes by long trajectories in the vicinity of the chaotic set. More precisely, the natural measure $P_i(\varepsilon)$ of nonempty box i is

$$P_i(\varepsilon) = \frac{N_i}{N}, \tag{1.12}$$

where N_i is the total number of trajectory points falling into box i. It is desirable to take N large enough that the condition $N_i \gg 1$ is satisfied in all nonempty boxes. The quantity $P_i(\varepsilon)$ is also called the *box probability* and represents the natural measure μ inside box i with an accuracy of order ε:

$$P_i(\varepsilon) = \int_{x \in \text{box } i} \mathrm{d}\mu(x). \tag{1.13}$$

Points of long-lived trajectories can be generated either by the ensemble, the sprinkler, or the PIM-triple method. An example of the natural measure of a chaotic saddle specified with finite resolution is shown in Fig. 1.10.

1.2.3.2 Conditionally Invariant Measure

A concept that is closely related to the natural measure is the c-measure introduced by Pianigiani and Yorke [595, 596]. For a nonattracting chaotic set, this measure is defined with respect to its unstable manifold. While there can be different c-measures for a given system [400], the "natural" c-measure is particularly relevant; it can be obtained as the *limiting distribution* of iterating trajectories starting from a *smooth* distribution of initial conditions about the chaotic set. In this sense, the c-measure is the analogue of the SRB measure [564] for attractors. For

transient chaos, the c-measure also describes how points *deviate* from the chaotic set, and can be regarded as being maintained by *supplying* new points into the region of interest according to the rate at which trajectories escape from the region asymptotically. Formally, this can be achieved by multiplying the number of points everywhere by the constant e^{κ} at each time step. Because of the contraction along the stable direction (if it exists), the limiting distribution will be nonzero *along the unstable manifold* only. This distribution, the c-measure, thus characterizes how points leave the neighborhood of the underlying nonattracting chaotic set asymptotically, and how often certain regions are visited by trajectories in the process of escaping. The natural measure μ can also be considered as the c-measure μ_c *restricted to* a small neighborhood of the nonattracting chaotic set itself.

Under the map $\mathbf{f}$, the region not escaping the restraining region Γ within one iterate is the preimage $\mathbf{f}^{-1}(\Gamma)$ of Γ. Since the c-measure characterizes how points are distributed along the unstable manifold before escaping, from a probabilistic point of view, it is the c-measure of $\mathbf{f}^{-1}(\Gamma)$ which is proportional to the number of trajectory points not escaping in one time step. By normalizing the c-measure of the restraining region to be unity, $\mu_c(\Gamma) = 1$, one finds, as pointed out by Pianigiai and Yorke [596], that the compensation factor is the reciprocal of $\mu_c[\mathbf{f}^{-1}(\Gamma)]$, i.e.,

$$e^{-\kappa} = \mu_c[\mathbf{f}^{-1}(\Gamma)]. \tag{1.14}$$

The escape rate is thus uniquely expressed by the c-measure of the nonescaping points within one iterate. Since the c-measure describes the asymptotic escape process, which is purely exponential, in choosing the density ρ_c of the c-measure as an initial density ρ_0 on Γ, the exponential form of the survival probability (1.8) is valid by the first time step. We see that ρ_c is thus the special initial distribution for which $n^* = 1$.

The c-measures of one-dimensional maps will be studied in detail in the next chapter. Here we briefly describe the construction of the c-measure for invertible two-dimensional maps. For such a system, the c-measure can be defined as follows [341]. Since trajectories escape the chaotic saddle along the unstable manifold, after $n \gg 1$ iterations, the surviving trajectory points of number N_n in Γ will be in the vicinity of the unstable manifold. Let B be a small box within Γ that contains part of the unstable manifold. The c-measure along the unstable manifold in B is thus

$$\mu_c(B) = \frac{N_{u,n}(B)}{N_n}, \quad \text{for} \quad n \gg 1, \tag{1.15}$$

where $N_{u,n}(B)$ is the number of the N_n points that fall in B at time n. An example of the c-measure is shown in Fig. 1.11. A comparison with the natural distribution in Fig. 1.10 indicates that the singular spikes of the c-measure fall outside the saddle, and that the natural distribution is nothing but the c-measure restricted to the saddle (with a proper normalization).

The natural measure μ of the chaotic saddle can also be defined based on $N_n^{(r)}(B)$, the number of trajectory points in B at a time rn between zero and n:

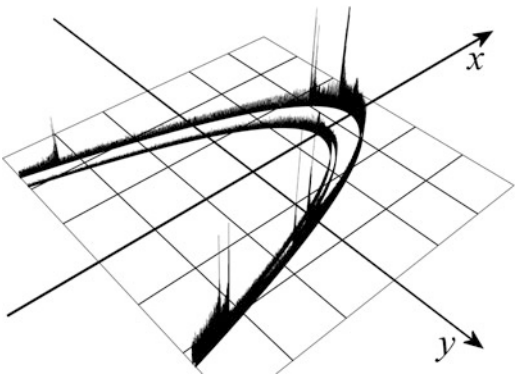

Fig. 1.11 Conditionally invariant measure μ_c of the Hénon saddle ($a = 2$, $b = 0.3$) on the restraining region $\Gamma : |x|, |y| \leq 1.5$, identified on a grid of size $\varepsilon = 1/400$. The support of the c-measure is the unstable manifold of the saddle (cf. Fig. 1.7) (Picture by M. Gruiz and Sz. Hadobás)

$$\mu(B) = \frac{N_n^{(r)}(B)}{N_n}, \quad \text{where } 0 < r < 1,\ n \gg 1. \tag{1.16}$$

We have $N_n^{(1)}(B) = N_{u,n}(B)$. For large N_0 and n, trajectories remaining in Γ will stay near the chaotic saddle for most of the time between zero and n, except at the beginning, when they are attracted toward the saddle along the stable manifold, and at the end, when they exit along the unstable manifold. Thus, the measure defined in (1.16) is independent of r, insofar as r deviates considerably from both 0 and 1.

A measure along the stable manifold can be defined as

$$\mu_s(B) = \frac{N_{s,n}(B)}{N_n}, \quad \text{for} \quad n \gg 1, \tag{1.17}$$

where $N_{s,n}(B)$ is the number of *initial conditions* in B whose trajectories do not leave Γ before time n (Fig. 1.12). Formally, this corresponds to evaluating (1.16) at $r = 0$. Measure μ_s can in fact be regarded as the c-measure of the time-reversed dynamics,[6] and a restriction of this measure to the saddle provides the natural measure of the saddle in the time-reversed dynamics. When plotting the measure of the two manifolds together, as in Fig. 1.13, one notes the following two features: (1) the singularities of the c-measure fall outside the saddle, an indication of the hyperbolic nature of the saddle, and (2) the restriction of the stable manifold measure to the saddle is different from the natural measure (Fig. 1.10, and red columns in Fig. 1.13). Both restricted measures are defined on the chaotic saddle, but they agree only if the dynamics is invariant under time reversal (e.g., as in Hamiltonian problems).

Note that the sprinkler method (Sect. 1.2.2.3) for the construction of the saddle and its manifolds is based on the concept of numbers $N_n^{(r)}$, and corresponds to the particular choice $r \approx 1/2$ for plotting points of the saddle.

[6] Because of the analogy between μ_c and μ_s, we can also call the conditionally invariant measure the measure of the unstable manifold.

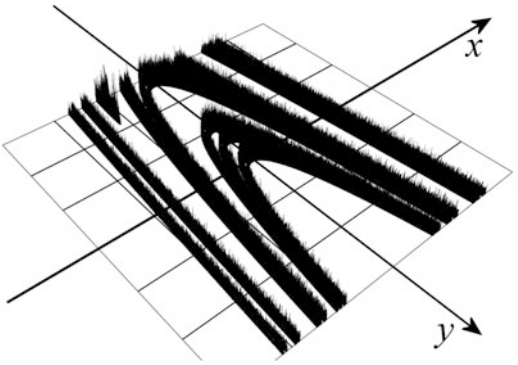

Fig. 1.12 Measure along the stable manifold (cf. Fig. 1.7) of the Hénon saddle for $a = 2$, $b = 0.3$, identified on a grid of size $\varepsilon = 1/400$. The region Γ is $|x|, |y| \leq 1.5$ (Picture by M. Gruiz and Sz. Hadobás)

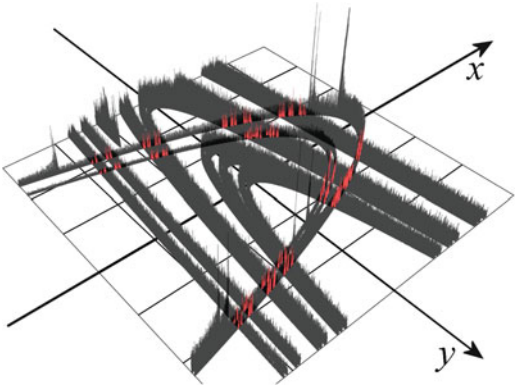

Fig. 1.13 Measure of the stable and the unstable manifolds. The natural measure of the Hénon saddle is shown in *red*. The distribution in *red* is the same as that of Fig. 1.10 but the spatial view is different. The restriction of the stable manifold's measure to the saddle differs from the natural measure. (Picture by M. Gruiz and Sz. Hadobás)

1.2.3.3 Characterization of the Natural Measure

Both the nonattracting set and its natural measure can possess complicated structures. To characterize the natural measure by certain numbers or simple functions is therefore of interest. In fact, such convenient characteristics are used widely in the study of chaotic attractors. While the characteristics can be worked out for *any type of invariant distributions* on the nonattracting set, we discuss here characterization of the natural measure, since it is physically most relevant. The typical characteristics are the Lyapunov exponents, the box-counting and information dimensions, the metric and the topological entropies, which are the dynamical invariants that we shall focus on in this book. For a more detailed analysis, full spectra of Lyapunov exponents, dimensions, and entropies can be introduced (see Appendix A). For simplicity we assume that there is only *one* expanding direction in the system. More-complicated cases will be treated in Chap. 8.

Consider first the *Lyapunov exponent*. Take a small interval of length Δ_0 along the unstable direction in a nonempty box i. It will be mapped after n steps onto a larger interval of some length Δ_n. The *stretching factor* Δ_n/Δ_0 can be written as $\exp[\Lambda_{1i}(n)]$, where the positive quantity $\Lambda_{1i}(n)$ is the *stretching exponent* belonging to box i. Here $\Lambda_{1i}(n)/n$ plays the role of a *local* Lyapunov exponent. The average

Lyapunov exponent λ_1 is simply the average of the stretching exponent with respect to the natural measure divided by n, i.e.,

$$\lambda_1 = \frac{1}{n}\sum_i \Lambda_{1i}(n) P_i(\varepsilon) \quad \text{for} \quad n \gg 1. \tag{1.18}$$

It should be noted again that the positivity of the Lyapunov exponent is not a defining characteristic for transient chaos, since any kind of nonattracting sets, e.g., unstable fixed points, can have a positive Lyapunov exponent. For an isolated saddle (hyperbolic) point one has, e.g., $\lambda_1 = \kappa > 0$.

The *fractal* properties of the nonattracting chaotic set and its natural measure describe how quantities scale with the box size ε. The box-counting dimension D_0 reflects how rapidly the number $N(\varepsilon)$ of nonempty boxes of dimensionless size ε covering the set increases with refining resolution:

$$N(\varepsilon) \sim \varepsilon^{-D_0} \quad \text{for} \quad \varepsilon \ll 1. \tag{1.19}$$

If the set is covered by boxes of different sizes ε_i, $i = 1,\ldots,N(\varepsilon)$, which are all bounded from above by an $\varepsilon \ll 1$, then (1.19) can be generalized to yield [45] the following implicit equation for D_0:

$$\sum_{i=1}^{N(\varepsilon)} \varepsilon_i^{D_0} = 1 \quad \text{for} \quad \varepsilon \ll 1. \tag{1.20}$$

This dimension characterizes only the geometry of the nonattracting set.

The *information dimension* is a measure of the inhomogeneity of the natural distribution. It measures how the information content of the box probabilities $P_i(\varepsilon)$ changes with the resolution:

$$-\sum_{i=1}^{N(\varepsilon)} P_i(\varepsilon)\ln P_i(\varepsilon) = D_1 \ln(1/\varepsilon) \quad \text{for} \quad \varepsilon \ll 1. \tag{1.21}$$

When the coverage consists of unequal small boxes of *different* sizes ε_i, but all bounded from above by some $\varepsilon \ll 1$, the information dimension D_1 can be expressed [45] by P_i, the probability that box i of size ε_i is visited, as

$$D_1 = \frac{\sum_i P_i \ln P_i}{\sum_i P_i \ln \varepsilon_i} \quad \text{for} \quad \varepsilon \ll 1. \tag{1.22}$$

The information dimension in fact belongs to a subset of the nonattracting set, the one that contributes dominantly to the information $-\sum_i P_i \ln P_i$. It therefore cannot be greater than the box-counting dimension:

$$D_1 \le D_0. \tag{1.23}$$

The equality holds only when the distribution is uniform: $P_i(\varepsilon) =$ constant on the nonattracting set.

Typically, one can associate a few symbols to different regions containing the nonattracting set, and assign a symbol when the trajectory visits a given region. This defines a *symbolic representation* of trajectories on the set [45,220,564]. By following trajectories of length m about the nonattracting set, one can specify how often a given symbolic sequence $\{S_j\}_1^m$ occurs. These *path probabilities* $P(\{S_j\})$ provide a complementary characterization of the chaotic set: entropies.

In particular, the *metric entropy* K_1 is defined as the growth rate of the information content of the path probabilities with length m of symbolic sequences [45, 220, 564]:

$$-\sum_{\{S_j\}} P(\{S_j\}) \ln P(\{S_j\}) = K_1 m \quad \text{for} \quad m \gg 1, \tag{1.24}$$

where the summation is taken over all symbolic sequences. Since the path probabilities depend on the natural measure, the metric entropy is also a characteristic of this measure. In terms of an information-theoretic interpretation [283], the metric entropy is the rate at which information stored in the insignificant digits of the initial condition flows toward the significant ones with time. The Lyapunov exponent λ_1 is in fact the mean velocity of this flow.

The *topological entropy* [2] K_0 reflects how complicated the organization of the symbolic encoding is: it is the growth rate of the number Ω_m of all allowed symbolic sequences of length m:

$$\Omega_m \sim \mathrm{e}^{K_0 m} \quad \text{for} \quad m \gg 1. \tag{1.25}$$

Here the different symbolic sequences are not weighted in terms of the path probabilities, whence the term "topological." The topological entropy can be also defined as the growth rate of the number N_m of all points of unstable periodic orbits of length m:

$$N_m \sim \mathrm{e}^{K_0 m} \quad \text{for} \quad m \gg 1. \tag{1.26}$$

A straightforward method for numerically calculating the topological entropy is due to Newhouse and Pignataro [548], which is based on the stretching of line segments in two-dimensional maps. Let L_n denote the length of the nth image of a line segment of initial length L_0 falling *within* some restraining region Γ enclosing the nonattracting set. One has

$$\frac{L_n}{L_0} \sim \mathrm{e}^{K_0 n} \quad \text{for} \quad n \gg 1. \tag{1.27}$$

Similar to the relation between the fractal and the information dimensions (1.23), we have the following inequality between the topological and the metric entropies [45]:

$$K_1 \leq K_0, \tag{1.28}$$

where the equality holds only for the special case in which all the symbolic sequences are equally probable.

An important feature of transient chaos is that there are exact and simple relations among the escape rate of the underlying nonattracting chaotic set, the information dimension, the Lyapunov exponents, and the metric entropy. In particular, one has

$$\kappa = g(\lambda_1, K_1) \tag{1.29}$$

and

$$D_1 = g_D(\lambda_1, K_1). \tag{1.30}$$

The particular forms of the right-hand sides of (1.29) and (1.30) depend on the dimensionality of the system. For maps of arbitrary phase-space dimensions, explicit expressions for g and g_D can be obtained, which we shall derive in later chapters.

Summarizing briefly, so far we have given, in terms of the quantities introduced, the criteria based on which the existence of a nonattracting chaotic set and consequently transient chaos can be established: (1) positivity of the topological entropy ($K_0 > 0$), and (2) fractality of the nonattracting set (noninteger values for the box-counting dimension D_0 or the information dimension D_1).[7]

That period three implies chaos [483], or equivalently, the existence of unstable cycles of infinite length, in fact implies the positivity of the topological entropy. It is then true that *period-3 implies transient chaos*.

1.3 Experimental Evidence of Transient Chaos

There has been ample experimental evidence of transient chaos. Here we shall present results from a few such experiments. In terms of quantification, earlier experiments mainly focused on determining the average transient lifetime, while more recent works have extended to characterizing the nonattracting chaotic set and its natural measure.

1.3.1 Convection Loop Experiment

The apparatus consists of a loop-shaped reservoir filled with water, which is heated from below along the lower semicircle and cooled from above, as shown in Fig. 1.14. The system was investigated from the point of view of chaotic dynamics by Widmann, Gorman, and Robbins [273, 274, 823], and by Bau and coworkers [822]. The system is the one-dimensional analogue of the Rayleigh–Bénard convection problem, and its dynamics can be described in certain parameter regimes

[7] The positivity of the largest Lyapunov exponent cannot be taken as a criterion because of the example of an isolated saddle point.

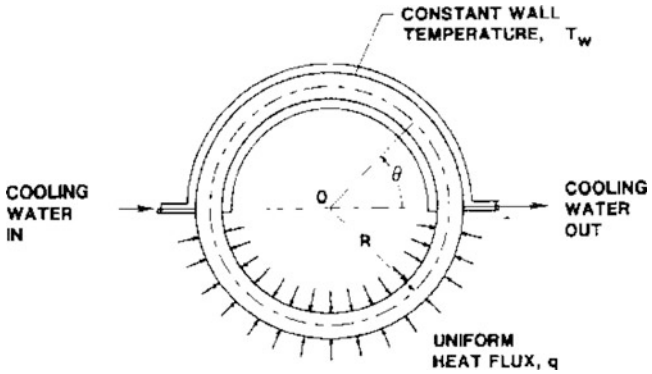

Fig. 1.14 Schematic diagram of the convection loop experiment. Representative results from the experiment are shown in Fig. 1.2 [823] (with kind permission from Elsevier Science)

by the Lorenz model [488]. After convection sets in at sufficiently high heat flux, the velocity of the fluid along the loop changes its sign and magnitude *in a chaotic manner*. There is a broad range of system parameters for which the chaotic oscillations last for a finite amount of time before settling into a state in which the system ceases to oscillate, as exemplified by Fig. 1.2. The duration of the transient chaotic oscillations depends sensitively on the initial state of the system.

1.3.2 Chemical Reactions Preceding Thermal Equilibrium

Stirred chemical reactions in closed containers cannot be chaotic in a sustained manner, since the system typically approaches thermal equilibrium after a transient period of time, corresponding to a fixed-point attractor in the space of the concentrations. Scott, Showalter and coworkers conjectured, however, that the *approach toward equilibrium*, i.e., the reaction dynamics before settling into the final fixed-point attractor, can be chaotic [700]. The conjecture was experimentally verified by Wang, Sorensen, and Hynne [820, 821] using the Belousov–Zhabotinsky reaction. Chaotic oscillations as the light transmission have been observed (Fig. 1.15) over several hours before a stage close to thermal equilibrium is reached.

1.3.3 Nuclear Magnetic Resonance Laser Experiment

The high quality of the data from an nuclear magnetic resonance (NMR) laser makes it appropriate for experimental investigations of a variety of chaotic phenomena. The laser output is a time-dependent voltage signal, and the control parameter is usually the modulation amplitude. At a bifurcation called a *crisis* (see Chap. 3), a chaotic

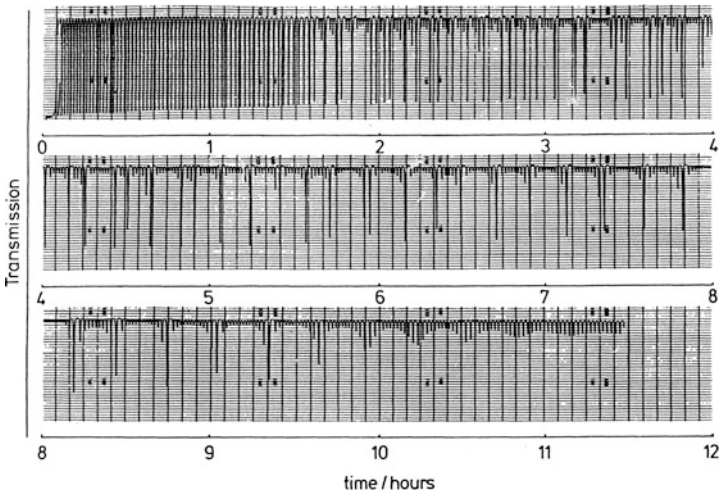

Fig. 1.15 Transiently chaotic oscillations (which start after about 1.5 h and continue for about 7 h) in a closed Belousov–Zhabotinsky reaction ending with small-scale oscillations that ultimately diminish as the system approaches thermal equilibrium [820] (Copyright 1994 by the American Chemical Society)

attractor undergoes a sudden explosion in its size. In particular, slightly before the crisis only a small-size attractor exists. In this regime, before settling into the small attractor, trajectories started from random initial conditions exhibit chaotic motion in the region where the postcrisis attractor lives, signifying transient chaos coexisting with permanent chaos. Time-series analysis of transient chaos [356] led to a successful reconstruction of the chaotic saddle responsible for the observed transient behavior, which was accomplished by considering only the parts of the signals that do not belong to the small attractor. By combining a number of such truncated signals, a long time series can be generated that is amenable to chaotic time-series analysis [382]. In this way, not only can the chaotic saddle be reconstructed, but also its dynamical characteristics, such as the average Lyapunov exponent, can be determined (Fig. 1.16).

1.3.4 Driven Pendulum

The parametrically driven damped pendulum is another example in which high-precision experiments [479, 480] on transient chaos can be carried out. In such an experiment, the angle and the angular velocity of the pendulum are measured, with the damping constant as a bifurcation parameter. The chaotic saddle can be reconstructed using a stroboscopic map. The experiment demonstrates, explicitly, fractality along both the stable and the unstable manifolds (Fig. 1.17). The box-counting dimension of the saddle was determined to be about $D_0 = 1.7$. For a more recent pendulum experiment, see [170]

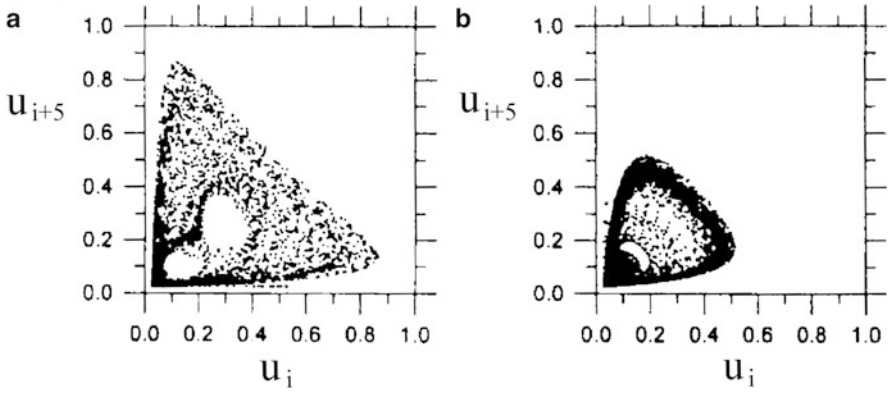

Fig. 1.16 Reconstruction of the chaotic sets from a nuclear magnetic resonance (NMR) laser experiment via time series analysis. (**a**) Chaotic saddle, (**b**) coexisting chaotic attractor. Note that the saddle not only appears larger, it is also more chaotic: its average Lyapunov exponent is about twice as large as that of the attractor [356] (Copyright 1994 by the American Physical Society)

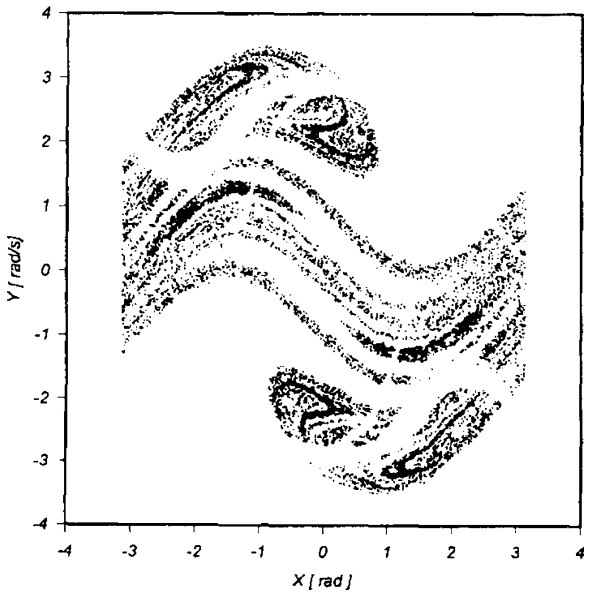

Fig. 1.17 A chaotic saddle reconstructed from the driven-pendulum experimental data. The double Cantor set character can be seen through the blank saps amid the points [480] (with kind permission from Elsevier Science)

1.3.5 Fractal Basin Boundaries

The boundaries between basins of attractions can often be fractal in nonlinear dynamical systems, and transient chaos can arise in a phase-space region containing such boundaries. Experimental observation of fractal basin boundaries can be quite

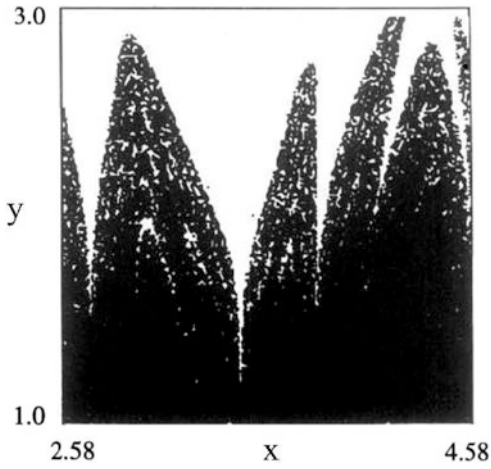

Fig. 1.18 For an electric circuit system of four coupled chaotic oscillators: basin of the synchronous chaotic attractor in *black*, and basin of one of the periodic attractors in *white*. The horizontal and vertical coordinates are proportional to the initial deviations of two coordinates of the oscillators from a point on their common chaotic attractor. Points of the white basin are dense in the black basin: the black basin is riddled [322] (copyright 1994, the American Physical Society)

challenging because of the necessity to choose initial conditions on a fine scale and to monitor each trajectory until it approaches one attractor. An experimental investigation of an extreme type of fractal boundaries is due to Heagy et al. [322], who studied a system of a set of four weakly coupled, nearly identical oscillators. Each isolated oscillator exhibits a chaotic attractor, and the attractor associated with the whole coupled system corresponds to a synchronous motion of the chaotic oscillators. The coupled system also possesses periodic attractors. Figure 1.18 shows the basins of the synchronized state (set of black points) and of one of the periodic attractors (white regions). The black basin exhibits a rather special property: it is the *riddled* basin where every point in the black basin has points of the white basin arbitrarily nearby.

1.3.6 Advection in the Wake of a Cylinder

In two-dimensional laminar flows around some obstacles, von Kármán vortex streets are typically formed. Due to the periodic detachment of vortices in the wake, the flow is periodic in time. The advection of particles is generally chaotic in time-periodic flows. In particular, since strong time-dependence is restricted to the wake only, advective chaos is transient, as illustrated in an experiment with a towed cylinder by Sommerer, Ku, and Gilreath [725]. The physical space of the fluid motion happens to coincide with the phase space, rendering directly observable fractal patterns that usually exist in the phase space. Of particular interest is the unstable manifold of the chaotic saddle in the wake, since dye particles flow away along this manifold. The experiment not only illustrated that dye (or pollution) often spreads out along fractal patterns, but also provided an example in which a fractal unstable manifold can be seen even by the naked eye, as shown in Fig. 1.19.

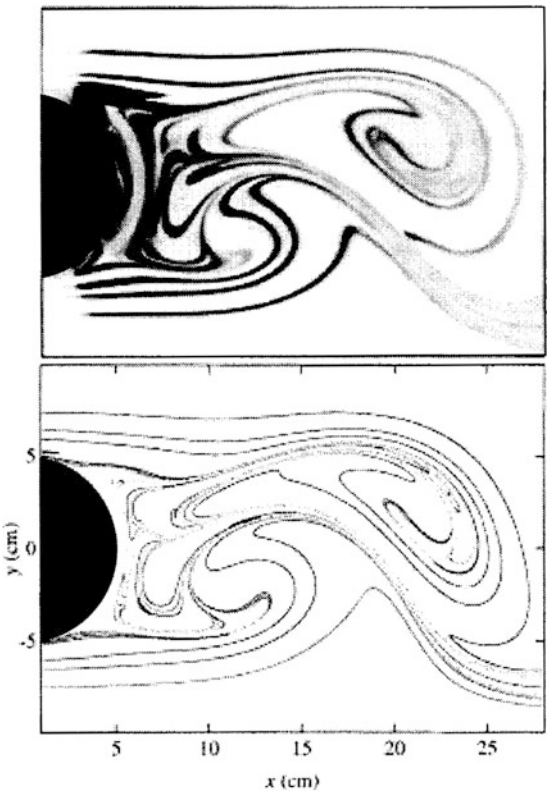

Fig. 1.19 For the experiment of advection in the wake of a cylinder (*black disk*), fractal pattern traced out by spreading a dye droplet the unstable manifold of a chaotic saddle existing in the wake. The flow is from left to right, and the droplet is injected into the upstream of the flow. The *lower panel* shows the results of a numerical simulation of the same problem [725] (copyright 1996, the American Physical Society)

1.3.7 Semiclassical Fluctuations in Chaotic Scattering

Interference effects of the scattering process become important in the semiclassical regime where wave properties are observable. Chaotic wave scattering, the scattering of waves from systems for which the underlying classical dynamics is chaotic, is observable not only in nanoscale electronic devices, but also in microwave scattering from macroscopic objects. Doron, Smilansky, and Frenkel [204] investigated the reflection of microwaves from an elbow-shaped cavity, where the underlying classical ray dynamics is chaotic with an exponential decay of rate κ in the survival probability of particles in the cavity. The basic quantity characterizing the wave-scattering process is the scattering matrix $S(\omega)$ as a function of the frequency. According to the semiclassical theory, the squared modulus of its Fourier transform $S(t)$ tends to decay with the *classical* escape rate κ. This is consistent with the experimental findings, as shown in Fig. 1.20. It can also be seen that the absolute value of the squared frequency-dependent autocorrelation function is a Lorentzian of half-width κ.

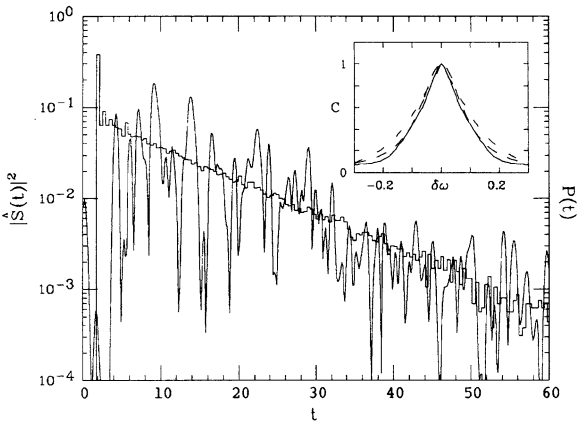

Fig. 1.20 For microwave scattering from an an elbow-shaped cavity, squared modulus of the time-dependent S-matrix, $|\, S(t)\,|^2$ (oscillating curve), exhibiting an overall decay that agrees with that of the classical escape-time distribution (curve in background). *Inset*: squared modulus of the frequency- (energy-) dependent autocorrelation function from the measured data (*continuous line*) and from the semiclassical theory (*dashed line*). The dimensionless half-width is $\kappa = 0.1$ [204] (copyright 1990, the American Physical Society)

1.3.8 Emission of Light from Dielectric Cavities

Dielectric cavities of cylindrical or spherical geometry are of technological importance because they can keep light trapped for a long time. When light circulates almost tangent to the surface of such a cavity via total internal reflection, it suffers minimal loss. Slightly deformed cavities emit light of nonnegligible intensity, and it was observed with surprise that these emissions are peaked in certain directions. A measurement by Schwefel and coworkers [699] records the light intensity for billiard-shaped cavities as a function of two angles: the angle Φ along the sidewall of the billiard, and an angle θ by which the camera is rotated in the far field from the major axis. Figure 1.21 shows the result for three different shapes with a deformation corresponding to approximately the same major-to-minor-axis ratio. Light intensity is localized to certain regions of the (Φ, θ) plane, meaning that light is emitted at specific points of the sidewall only, and in an approximately predetermined direction. Although the billiard shapes (shown as insets) appear similar in the last two cases, the emission patterns are rather different: the intensity integrated over the sidewall angle is peaked, e.g., about 90° and 30°. In the geometrical optics approximation, the patterns can be explained by the existence of a chaotic saddle of exceptional light rays that are never transmitted, i.e., they are subject to permanent total internal reflection both forward and backward in time. The form of these saddles depends sensitively on the shape of the billiard. In addition, the directionality of the light has been shown to be intimately related to the unstable manifold of

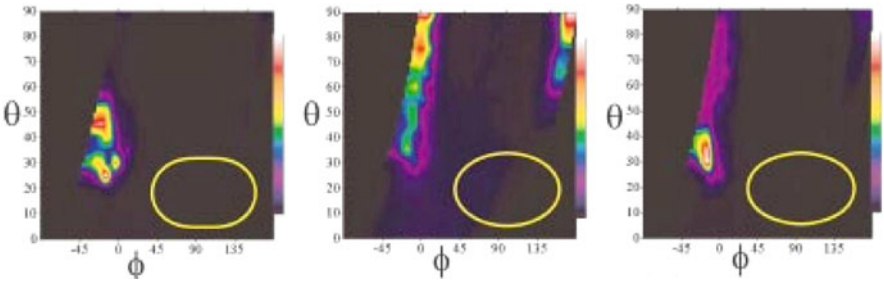

Fig. 1.21 Light emission intensity in false color (*color bar* at the sides) as a function of the sidewall angle Φ and of the camera angle θ for three microcavities, whose shapes are drawn as insets [699] (copyright 2004, the Optical Society of America)

certain unstable fixed points [699], and more rigorously, of the entire chaotic saddle [15]. This is thus a further example in which the unstable manifold of chaotic saddle become related to physical observables.

1.3.9 Maintaining Chaos in a Magnetoelastic Ribbon

Since there are systems that require chaos in order to function properly, it is important that transient chaos be convertible into permanent chaos. The aim of this procedure, which is called *maintenance of chaos*, is to intervene in the dynamics in such a way as to keep chaotic behavior alive in situations in which it would naturally be absent. A possible realization is to apply properly chosen perturbations to the signal in order to keep it always on that side of the stable manifold of a hyperbolic point from which a return to a nonattracting chaotic set is allowed. The method can be improved by finding a target point on this side from which a transiently chaotic trajectory of long lifetime is initiated, and trying to direct the signal to the target point [697]. In an experiment by In et al. [351], chaos in a magnetoelastic ribbon was successfully maintained at a parameter set where a fixed-point attractor exists; see Fig. 1.22. The quantity X_n plotted is proportional to the position of a point on the ribbon measured once every driving period of an applied external magnetic field.

1.3.10 Turbulence in Pipe Flows

In a pipe flow, a steady laminar solution is linearly stable for *all* Reynolds numbers $Re \equiv UD/\nu$, where U is the average velocity in a pipe of diameter D, and ν is the kinematic viscosity. The turbulent state can be considered as a high-dimensional chaotic state associated with a chaotic saddle. In an experiment, Peixinho and Mullin followed turbulent puffs downstream and measured their positions along the pipe

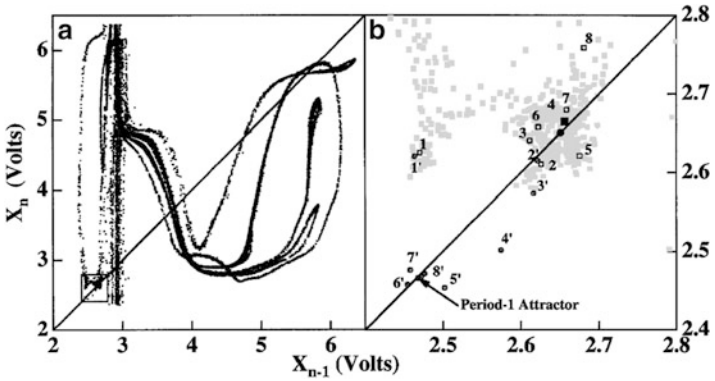

Fig. 1.22 Maintaining chaos in an experiment by In et al. [351]. (**a**) Projection of the stabilized chaotic attractor. (**b**) Blowup of the square shown in (**a**). The *filled circle* on the diagonal marks the hyperbolic point and the *filled square* marks the target. *Small circles* 1′–8′ show an unperturbed sequence and *small squares* 1–8 illustrate the perturbed sequence (Copyright 1998, the American Physical Society)

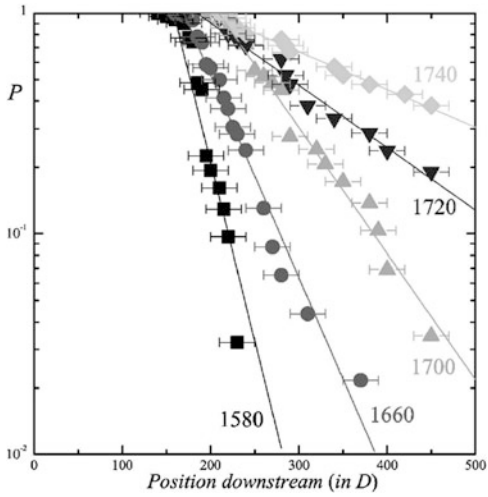

Fig. 1.23 For an experiment of turbulence in a pipe flow, probability of observing a turbulent puff as a function of the dimensionless downstream distance from the point where the puff is generated. The numbers associated with different experimental curves denote the Reynolds number *Re*. It can be seen that the escape rate decreases with *Re* [589] (Copyright 2006, the American Physical Society)

where the puffs are relaminarized [589]. The distributions exhibit exponential decay, as shown in Fig. 1.23. Normalized by length D and time D/U, the dimensionless distance and the dimensionless time to reach this distance are proportional to each other, i.e., the dimensionless velocity is of the order of unity. Turbulence in pipe flows is thus a high-dimensional chaotic transient with finite lifetime. Recent investigations indicated that the average lifetime tends to grow extremely rapidly with the Reynolds number [334, 336].

1.4 A Brief History of Transient Chaos

The first observation of chaotic transients was part of the prehistory of chaos science. In the late 1940s, in their early studies of the forced Van der Pol oscillator, Cartwright and Littlewood [114] and Levinson [482] found signatures of chaotic transients as the system settles into one of the coexisting attractors (there are in fact fractal basin boundaries between the basins of attraction). Later, in 1973, Chirikov and Izraelev identified certain transient features in weakly dissipative systems [134, 135].

A systematic investigation of transient chaos began in the late 1970s with the works of Shimizu and Morioka [714], Kaplan and Yorke [386], and Yorke and Yorke [843] on the dynamics of the Lorenz system in parameter regimes that differ from the standard one with a chaotic attractor, where the attractors are either limit cycles or fixed points. An important step toward a firm mathematical foundation of the phenomenon was the introduction of the concept of the conditionally invariant measure by Pianigiani and Yorke [595, 596]. Subsequently, several theoretical papers reported this phenomenon in all kinds of nonlinear systems: low-dimensional maps [141, 184, 500], nonlinear oscillators [337, 338, 512], systems modeled by time-delayed equations [380], partial differential equations [348, 715], and coupled oscillators [795].

A comprehensive investigation of transient chaos originated from the discovery that chaotic transients arise typically in systems passing through a type of global bifurcation called crisis (Grebogi, Ott, and Yorke in 1983 [293]). The Maryland Chaos Group has played since then an important role in the understanding of further transient-chaos-related phenomena, which include fractal basin boundaries, Wada boundaries [406, 780], and riddled basins [11]. The importance of the natural measure on nonattracting chaotic sets and of quantities related to it was pointed out by Kantz and Grassberger in 1985 [380] and later by Hsu, Ott, and Grebogi [73, 341], generating further interest in the topic (see reviews in [766] and [770]).

Interest in the chaotic aspects of scattering processes dates back to early studies of classical chemical reactions [56,275,555,622] and point–vortex interactions [25]. A systematic study of the subject began in the late 1980s with the work of Jung [360], Eckhardt [210, 211], Hénon [326], and Bleher, Ott, and Grebogi [73, 74]. The concept of chaotic advection, coined by Aref [26] and generalized to open hydrodynamical flows, corresponds to a transiently chaotic spreading of particles [371]. This is in fact a chaotic scattering process, which has important applications in pollutant transport. The quantum-mechanical aspects of chaotic scattering were addressed by Blümel and Smilansky [76], Jung [368], Gaspard and Rice [259], and Cvitanović and Eckhardt [152].

The work by Crutchfield and Kaneko [146] on transient chaos in spatiotemporal systems generated a new perspective of research aiming at understanding whether spatiotemporal complexity, or turbulence, is related in general to attractors or rather to nonattracting chaotic sets generating long-lived transients.

The first experimental indications of irregular transient behavior were found in hydrodynamical systems, where transients were followed over days before

settling down on a periodic attractor [9]. Although in current terminology these were spatiotemporal chaotic transients, a number of papers appeared afterward reporting low-dimensional transiently chaotic behavior in systems exemplified by a compass forced by a magnetic field [145], lasers [23,154,577], electronic oscillators [22,333,646], and a parametrically forced pendulum [479]. Besides the convection-loop [273,274] and the pendulum [479,480] experiments (cf. Sect. 1.3), a spin-wave experiment [110, 111, 113] seemed to have provided high-quality measurements of chaotic transients. Other investigations included the dynamics of a bouncing ball [422] and a driven magnetoelastic ribbon [196]. Many experimental systems in which transient chaos has been observed are in fact systems with fractal basin boundaries (e.g., [22, 422, 577]). In spite of these experimental works and the several experiments carried out in the last 20 years, it is possible that due to the limited awareness of the phenomena of transient chaos even among researchers in the nonlinear-dynamics community, transiently chaotic signals were considered to be uninterpretable and were discarded.